DETERMINING THE GENOTYPE-PHENOTYPE RELATIONSHIP OF *atg18a* MUTANTS

by

Matthew D. Fischer

A thesis submitted to the Faculty of the University of Delaware in partial fulfillment of the requirements for the degree of Degree of Science in Biological Sciences with Distinction

Spring 2015

DETERMINING THE GENOTYPE-PHENOTYPE RELATIONSHIP OF *atg18a* MUTANTS

by

Matthew D. Fischer

Approved: _____
Dr. Erica M. Selva, Ph.D
Professor in charge of thesis on behalf of the Advisory Committee

Approved: _____
Dr. Jia L. Song, Ph.D
Committee member from the Department of Biological Sciences

Approved: _____
Dr. Emily S. Day, Ph.D
Committee member from the Board of Senior Thesis Readers

Approved: _____
Michelle Provost-Craig, Ph.D.
Chair of the University Committee on Student and Faculty Honors

ACKNOWLEDGMENTS

When I matriculated as a student at the University of Delaware, I had declared Music Education as my major. It was not until I had an epiphany the summer before my undergraduate career started that I had a change of heart and considered studying the sciences. While I was not certain of what the future held, I ended up changing my major to Biological Sciences by the time the Fall 2011 semester started with the ambition of becoming a researcher of genetics. Looking back as a soon-to-be graduate, I have absolutely no regrets with changing my life goals so dramatically, and this is largely because of the extremely positive experiences I have had as both a student and researcher of molecular biology and genetics. I would like to take the time to give several people the appreciation they deserve for being so beneficial to my life.

First I would like to extend my highest gratitude to Dr. Erica M. Selva. It has been an absolute honor and joy to be introduced to research in your lab and learn the way of the fly. You have provided me with both intellectual and emotional guidance for the past two years, and I'm so very glad to have worked closely with you. Additionally, I would like to thank the whole lab: Brooke, Morgan, Erica S., Sencer, Kelly, Net, Katie, and John. It has been a pleasure both to work and have fun with all of you! I'll miss you all! I would also like to thank my committee members Dr. Jia Song and Dr. Emily Day, for they have been highly beneficial to the completion of this thesis. A special shout-out to my other friends and family who have always shown their love and support explicitly! Finally, I would like to thank the University of Delaware Undergraduate Research Program and Howard Hughes Medical Institute.

TABLE OF CONTENTS

LIST OF TABLES

LIST OF FIGURES

ABSTRACT

Autophagy is a process where cytoplasmic components are engulfed by a phagophore, which then fuses with lysosomes to degrade its contents. This is a highly regulated and conserved process that is active during conditions of starvation and normal cellular maintenance. 8J16 and 9E6 are two independent allelic point mutations in *Drosophila melanogaster autophagy-specific gene 18a* (*atg18a)* located in introns three and four, respectively, of its five exon locus at 66B11 on chromosome 3. These *atg18a* alleles were initially characterized as being involved in Wnt or Hedgehog signaling due to their embryonic phenotype. The $atg18a^{8J16}$ and $atg18a^{9E6}$ intronic mutations are not in any sequences expected to disrupt transcriptional processing, yet these mutations cause lethality in homozygous germline clone embryos, pupal lethality in deletion heterozygotes, and neurodegenerative phenotypes. $atg18a^{8J16}$ and $atg18a^{9E6}$ mutants also show an unusual cold sensitive phenotype and are temperature permissive when reared at an elevated temperature. This is not observed in a third adult lethal allele, $atg18a^{P}$, a P-element insertion of the construct *KG03090* in the 2nd exon (5' UTR) of *atg18a*. The exact molecular effects of these mutations are unknown. The purpose of this research is to investigate and determine the genotype-phenotype relationship of how $atg18a^{8J16}$, $atg18a^{9E6}$, and $atg18a^{P}$ alleles give rise to *atg18a* loss of function and characterize the effect of these mutations on neuronal maturation using the *Drosophila* eye as a model. Effects on splicing were examined by performing RT-PCR using primers that span introns of total RNA isolated from $atg18^{P}/\Delta DF4408$, $atg18^{8J16}/\Delta DF4408$, $atg18^{9E6}/\Delta DF4408$, and wild type

pupae. This analysis revealed no significant splicing defect, but a small effect was observed in *atg18*^{9E6}, which will be re-examined in the future. In adults, *atg18*^{8J16} and *atg18*^{9E6} homozygous mutant eyes are small and display the rough eye phenotype. To better understand the basis of this phenotype, mutant larval imaginal eye discs were examined to determine ommatidial organization and photoreceptor identity. ELAV, a pan-neuronal marker, showed that photoreceptors differentiate normally, but those that differentiate early are being lost. Examination of cleaved caspase 3 revealed that homozygous mutant photoreceptor cells were succumbing to apoptosis. It also showed significant death at the morphogenetic furrow and posterior compartment, which might result in a smaller pool of photoreceptor progenitors. Both of these phenotypes could contribute to the adult small, rough eye phenotype. These results suggest autophagy may be required for photoreceptor maintenance and its absence leads to apoptotic death. Examination of Senseless and Prospero expression showed that photoreceptors R8 and R7, respectively, are more refractory to apoptosis as these photoreceptors predominate near the optic stalk where the first photoreceptors differentiate. This suggests autophagy is more important for the maintenance of photoreceptors R1, R2, R3 R4, R5 and R6 than it is for R7 and R8.

Chapter 1

INTRODUCTION

1.1 The 8J16 and 9E6 Mutants

8J16 and 9E6 are two independent allelic point mutations in *Drosophila melanogaster autophagy-specific gene 18a* (*atg18a)* located in introns three and four, respectively, of its five exon locus at 66B11 on chromosome 3. These *atg18a* alleles were initially characterized as being involved in Wnt or Hedgehog signaling due to their 'lawn of denticle' cuticle embryonic phenotype (Figure 1; Selva & Stronach, 2007). The $atg18a^{8J16}$ and $atg18a^{9E6}$ intronic mutations are not located in any sequences expected to disrupt transcript processing, as predicted by bioinformatics analysis, yet these mutations cause lethality in homozygous germline clone embryos, late larval/early pupal lethality in deletion heterozygotes, and neurodegenerative phenotypes. The long-term goal of this project is to elucidate the genotype-phenotype relationship of these intronic mutations to identify the underlying molecular mechanism causing the phenotypes.

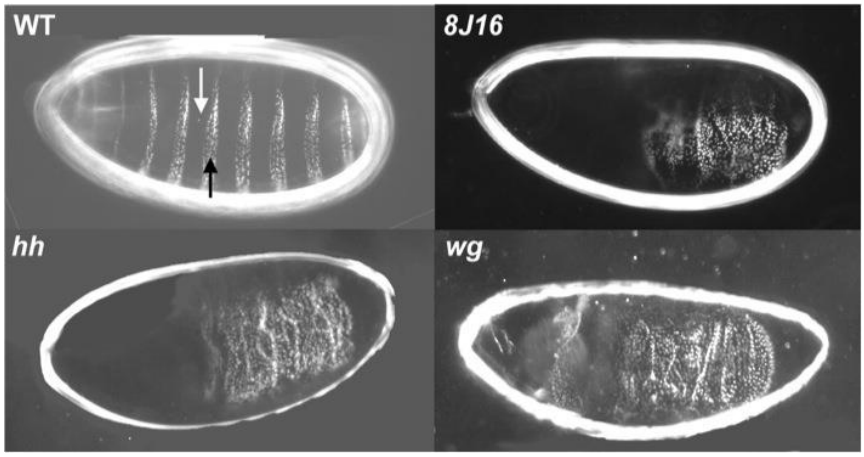

Figure 1. **Comparison of the 8J16 terminal embryonic cuticle phenotype to Hh and Wg mutants.** Hh and Wg signaling pathways are required for the deposition of naked cuticle (white arrow in wild type, WT) in the embryo. Black arrow indicates denticle bands. Mutations that disrupt either pathway yield a 'lawn of denticles' phenotype. The 8J16 and 9E6 mutations yield the same 'lawn of denticles' phenotype, suggesting they disrupt Hh or Wg signaling. Images are taken in darkfield with the vitelline membranes intact (Figure adapted from Selva & Stronach, 2007).

1.2 Autophagy

Autophagy is a process of generalized cellular recycling which involves the sequestration of cytoplasmic contents in a phagophore and subsequent degradation to constitutive monomeric macromolecules proceeding fusion with a lysosome (Feng *et al.*, 2014). These monomers are then released from the double membrane structure into the cytosol for reuse for nutritional or anabolic processes to survive cellular stress states, such as starvation or heat shock.

Autophagy begins with the induced assembly of the double-membrane phagophore within the cytoplasm at the phagophore assembly site (PAS). When this phagophore completes its expansion and encloses around cytoplasmic contents, it has become the autophagosome. This structure then fuses with the late endosome (vacuole

in yeast). Subsequent fusion with a lysosome exposes the contents of the now autophagolysosome to hydrolases and other degradative enzymes, catabolizing the contents into their constitutive macromolecular monomers (Figure 2; Feng *et al.*, 2014).

The process of autophagy depends on the functions of the core autophagic molecular machinery's five components, each of which consists of *autophagy-related gene* (*atg*) proteins (Figure 3). These are the Atg1/ULK complex, Atg9 and its cycling system, the phosphotidyl inositol (PtdIns3K) complex, the Atg8 Ubl conjugation system, and the Atg12 Ubl conjugation system (Feng *et al.*, 2014). Each of these sub-processes carries out a function necessary to autophagy; the Atg1/ULK complex (Atg1, Atg11, Atg13, Atg17, Atg29, and Atg31) mediates autophagosome formation (Feng *et al.*, 2014). Atg9 and its cycling system (Atg2, Atg9, and Atg18) are involved in delivering membrane to the expanding phagophore following the initial activities of the Atg1/ULK complex (Feng *et al.*, 2014). The PtdIns 3-kinase complex (Vps34, Vps15, Vps30/Atg6, and Atg14) recruits PtdIns3P-binding proteins to the PAS by generating phagosomal phosphatidylinositol 3-phosphate (PI3P; Feng *et al.*, 2014). The final two components, the Atg12 (Atg5, Atg7, Atg10, Atg12, and Atg16) and the Atg8 (Atg3, Atg4, Atg7, and Atg8) conjugation systems, are involved in vesicle expansion (Feng *et al.*, 2014). All of these Atg proteins are necessary for the proper formation of the autophagosome, and deficiencies in any of them result in a disruption to autophagy. Though the molecular mechanisms of autophagy have been largely studied in *Saccharomyces cerevisiae*, it has been shown that autophagy is an evolutionarily conserved process from yeast to humans, including *Drosophila melanogaster* (Feng *et al.*, 2015).

Since its discovery during the 1960's, it has been elucidated that autophagy is involved in a number of biological processes. These include immunity, starvation-survival, homeostatic regulation, and development (Feng *et al.*, 2014). While the manner by which autophagy regulates development remains unclear, work by Lorincz *et al*. has shown that the function of the PtdIns 3-kinase complex is modular and unique depending on with which of two regulatory proteins, Atg14 or the ultraviolet radiation resistance associated (UVRAG), it is associated (2014).

If the complex's components are associated with Atg14, then the complex's catalytic activity is directed towards phagosomal PI3P generation. This is a requirement for the creation of the phagophore and the autophagosome. Atg14 thus bestows upon the PtdIns 3-kinase autophagy-regulating properties (Lorincz *et al.*, 2014).

The other regulatory protein for the PtdIns 3-kinase complex is the UVRAG protein, and the complex's association with this directs its catalytic activity towards endosomal PI3P generation and endosomal maturation (Lorincz *et al.*, 2014). Furthermore, Lorincz *et al.* show that the UVRAG-associated complex is necessary for endocytotic regulation and is involved in receptor maintenance. This includes regulation of developmental receptors such as Notch, connecting the functionalities of one of the autophagy's core molecular machinery with development. Additionally, they show that the UVRAG-associated PtdIns 3-kinase complex is involved in regulation of the paracrine factor Wingless, the primordial *Drosophila* Wnt (2014). Specifically, Lorincz *et al.* demonstrated that the UVRAG-associated PtdIns 3-kinase complex is required for the proper regulation of Wingless signaling during *Drosophila melanogaster* wing disc development (2014). Interestingly enough, while *atg14*

mutants displayed phenotypes indicative of a disruption to autophagy, these cells did not display a phenotype indicative of disrupted Wnt signaling. This suggests that while components of the core autophagic machinery may be involved in processes other than autophagy, the process of autophagy itself is not necessarily correlated to the regulation of Wingless signaling.

atg18a is a 3,714 base pair, protein-coding gene located on chromosome 3 within cytological region 66B11. It is composed of four introns and five exons. 8J16 and 9E6 are both intronic point mutations and have been identified using comprehensive complementation analysis (Figures 4 and 5). The specific mutations were found by sequencing genomic DNA from adult heterozygotes that harbor these mutations. These *atg18a* mutations also cause severe nervous system defects, including but not limited to a rough eye phenotype when homozygous in the eye (Figure 6). The exact molecular function of *atg18a* in nervous system development and/or degeneration is currently unknown. Interestingly, 8J16 and 9E6 mutants are cold-sensitive and show viability when reared at an elevated temperature (Table 1).

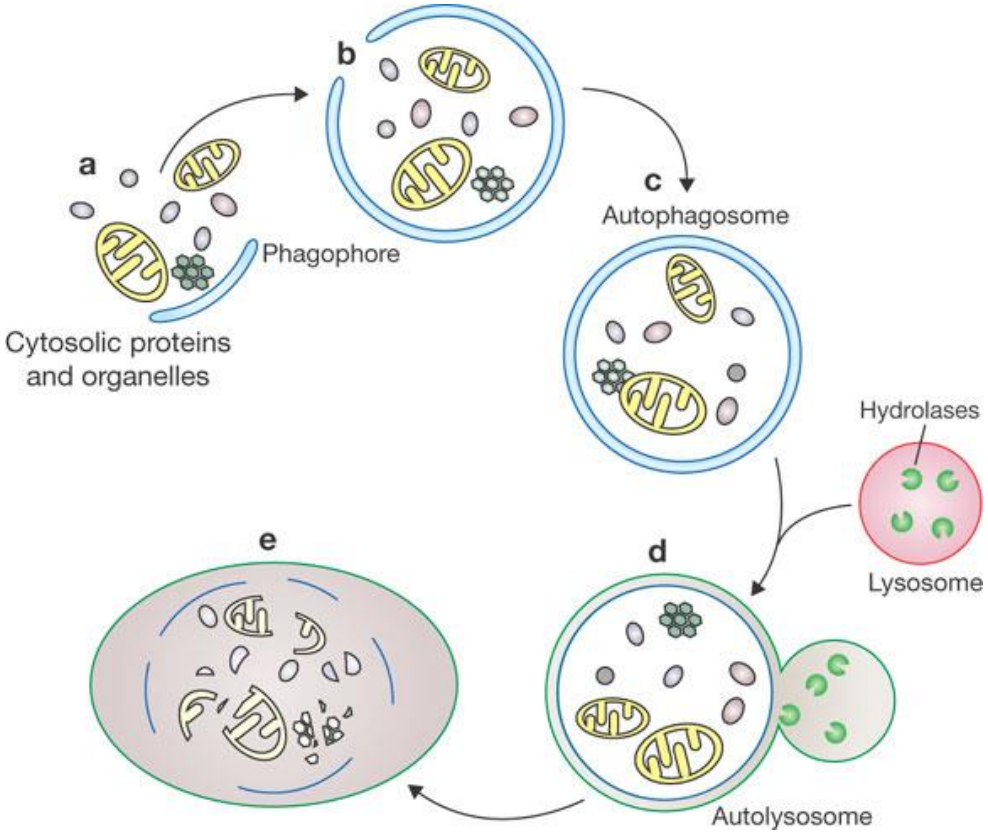

Figure 2. **The process of autophagy.** (**a**, **b**) Cytosolic material is sequestered by an expanding membrane sac, the phagophore (**c**) resulting in the formation of a double-membrane vesicle, an autophagosome (**d**) the outer membrane of the autophagosome subsequently fuses with a lysosome, exposing the inner single membrane of the autophagosome to lysosomal hydrolases (**e**) the cargo-containing membrane compartment is then lysed, and the contents are degraded (Figure adapted from Xie and Kilonsky, 2007).

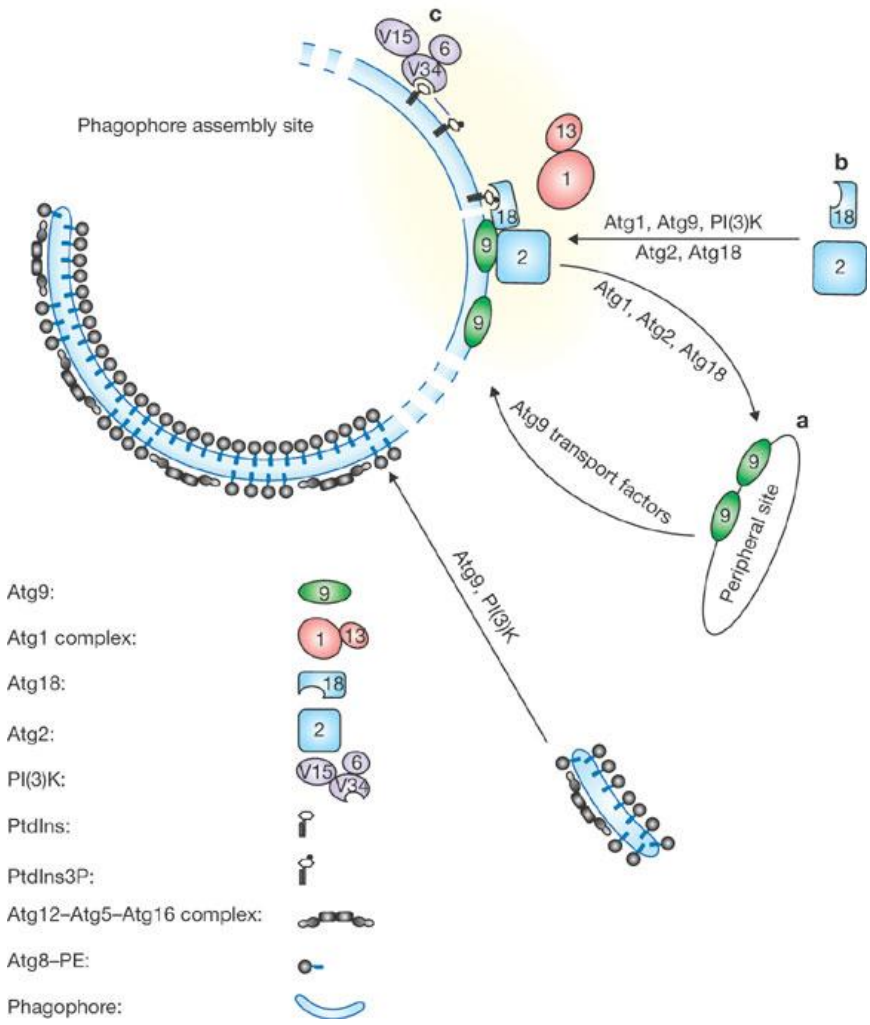

Figure 3. **Autophagy's core molecular machinery and the phagophore assembly site (PAS).** Atg1/ULK complex (Atg1, Atg11, Atg13, Atg17, Atg29, and Atg31) mediate autophagosome formation. Atg9 and its cycling system (Atg2, Atg9, and Atg18) are involved in delivering membrane to the expanding phagophore following the initial activities of the Atg1/ULK complex. The PtdIns 3-kinase complex (Vps34, Vps15, Vps30/Atg6, and Atg14) recruits PtdIns3P-binding proteins to the PAS by generating phagosomal phosphatidylinositol 3-phosphate (PI3P). The final two components, the Atg12 (Atg5, Atg7, Atg10, Atg12, and Atg16) and the Atg8 (Atg3, Atg4, Atg7, and Atg8) conjugation systems, are involved in vesicle expansion (Figure adapted from Xie and Kilonsky, 2007).

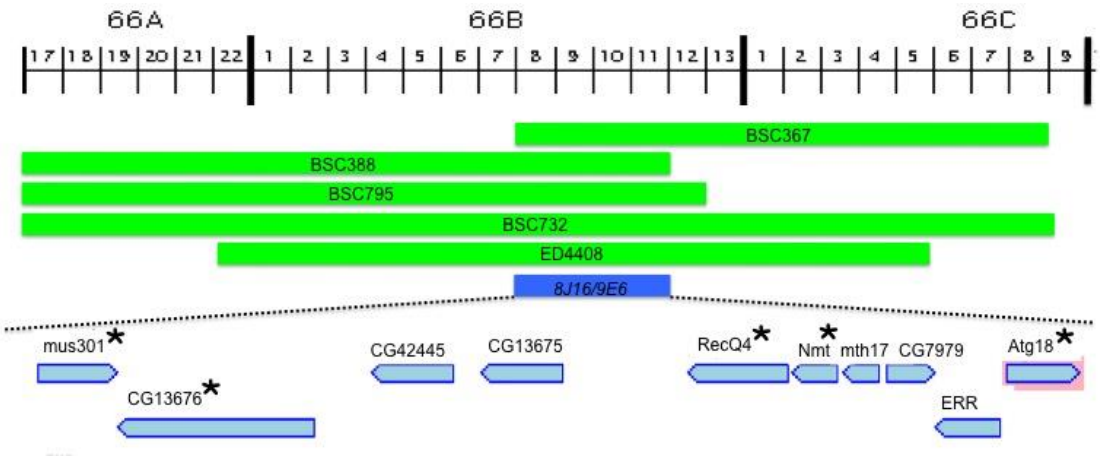

Figure 4. **Complementation analysis delineating the discovery of *atg18* as the gene disrupted by 8J16 and 9E6 mutations.** Regions absent in deficiencies are shown as solid bars. Green denotes non-complementation, therefore 8J16/9E6 are between 66B8 and 66B11 on the left arm of chromosome three, the region of overlap. Mutants did complement BSC815 (not shown), a deficiency just outside of this region. Complementation analysis to mutants in five of the ten genes within this region (marked with asterisks) identified 8J16 and 9E6 as two novel alleles of *atg18*. An independent mutation in *atg18* did not complement the 8J16 or 9E6 mutations (Figure adapted from Boetefeur, 2012).

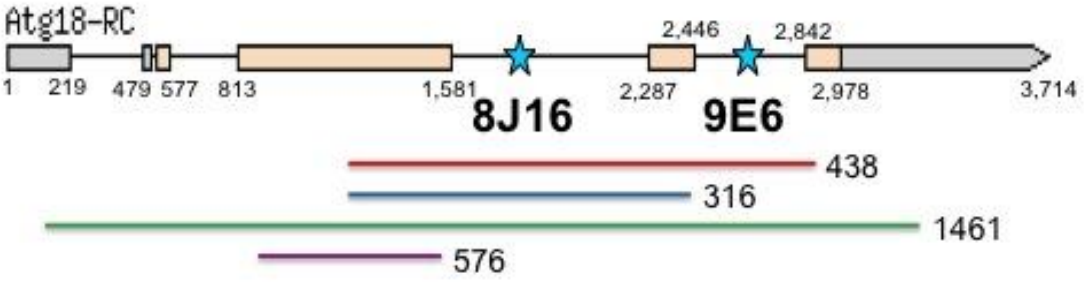

Figure 5. **8J16 and 9E6 *atg18* intronic point mutation and location of primers that will be used to examine possible splicing defects.** Colored bars correspond to the products of primer pairs of unspliced *atg18* message. Numbers listed to the right of each bar are the expected fragment size for each primer pair. The purple bar represents an internal control primer pair, located within the first major exon and is not predicted to be affected by the 8J16 or 9E6 mutation (work done by Boetefeur, 2012).

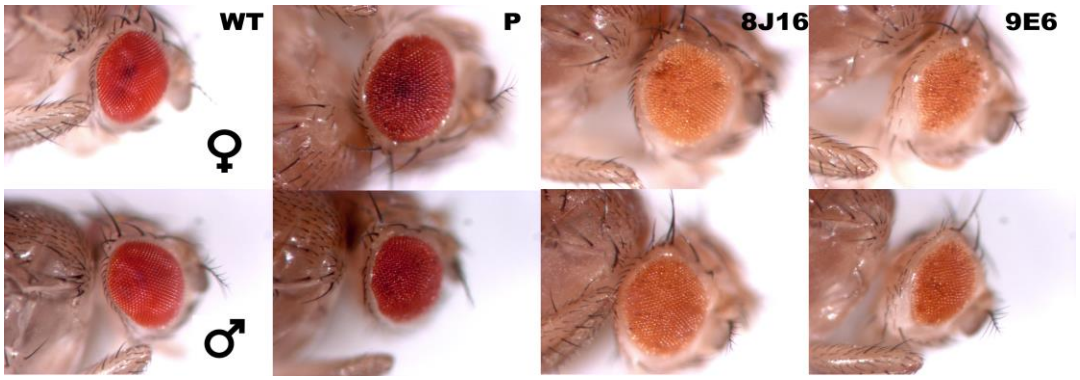

Figure 6. **Allelic series of *atg18* mutants**. *Drosophila* with genotypes *atg18*$^{P\ FRT\ 2A}$/TM3, 8J16$^{FRT\ 2A}$/TM3, and 9E6$^{FRT\ 2A}$/TM3 were crossed with ey^{flp};gmr-hid$^{FRT\ 2A}$/SM5_TM6B, producing offspring with homozygous mutant eyes. The mutations were then aligned in order of neurodegenerative phenotypic severity in regard to the eye of the fly. This series visually portrays the severity of the mutations' other phenotypic effects.

Table 1: **8J16 and 9E6 show complete rescue at 29°C.** When crossed with flies deficient for the atg18 gene region, the expectation is that 33% of the pupal offspring will be of the genotype mutant/null, marked by the absence of the tubby marker, TM6B. This number is greatly reduced in 8J16 and 9E6 at room temperature (~25°C) but rescued at the elevated temperature, 29°C. The same observation is not made with atg18aP.

Cross	RT (~26°C)	% Tb^+	29°C	% Tb^+
♀ atg18^P/TM6B,Tb x ♂ED4408/TM6B,Tb	52 Tb^+ 101 Tb^-	34.0%	67 Tb^+ 158 Tb^-	29.8%
♀ 8J16/TM6B,Tb x ♂ED4408/TM6B,Tb	14 Tb^+ 112 Tb^-	11.1%	82 Tb^+ 127 Tb^-	39.2%
♀ 9E6/TM6B,Tb x ♂ED4408/TM6B,Tb	26 Tb^+ 94 Tb^-	21.7%	46 Tb^+ 84 Tb^-	35.4%

1.3 Ommatidial Development and Organization

The compound eye of *Drosophila melanogaster* is a highly organized structure. It consists of 800 neuronal clusters organized into 32 interlocking columns in units known as ommatidia. The ommatidium is formed of eight photoreceptor neurons (R1-R8), four lens-secreting cone cells, and two primary pigment cells. Additionally, adjacent ommatidia share six secondary pigment cells, three tertiary pigment cells, and three mechano-sensory bristle complexes (Kumar, 2012).

Ommatidial development and neuronal specification is an invariant process and is highly consistent between individual *Drosophila*. The proper functionality of the compound eye is heavily reliant upon this invariance, for a rough eye phenotype can be observed if the cluster is missing even one neuron (Kumar, 2012).

The adult compound eye arises from the larval imaginal eye-antennal disc. This disc is formed during embryogenesis as an eight cell structure. These cells undergo a multitude of divisions throughout the first two larval instars, dividing the disc into the dorsal and ventral compartments. Eye fate rather than antennal fate is specified by the retinal determination network (Kumar, 2012).

Between the end of the second larval and third larval instars, a morphogenetic furrow initiates at the posterior end of the eye disc and traverses anteriorly (Figure 7). Paracrine factors are secreted from this furrow, and this results in a wave of differentiation by which photoreceptor fate is determined and differentiated (Kumar, 2012).

Morphogenetic development initiates with the formation of periodic rosette structures, which are clusters of approximately 20 cells organized by the furrow. Several cells are expelled from the cluster until a structure of seven to nine cells remain, giving rise to the five-cell precluster. The expelled cells undergo one round of

mitosis, and some of the produced daughter cells immediately reassociate with the precluster (Kumar, 2012).

The order of photoreceptor differentiation is genetically coordinated and for the most part occurs in pairs. R8 is the first photoreceptor to differentiate, followed by the R2/5 pair, proceeded with the R3/4 pair, and concludes with the R1/6/7 triplet (Kumar, 2012).

R8 fate is determined by the expression pattern and activity of *atonal* (*ato*), a gene which encodes a transcription factor. Ato protein is expressed by periodically spaced clusters of 10-15 cells of the rosette. Notch signaling represses *ato* transcription and refines this expression to the equivalence group (the presumptive R8/2/5 photoreceptor cells comprised of three cells of the five-cell precluster). A regulatory network involving the Rough and Senseless proteins ultimately resolves *ato* expression to the presumptive R8 photoreceptor cell. The *rough* gene encodes a homeobox DNA binding protein, and its expression is restricted by the morphogenetic furrow to the presumptive R2/5 and R3/4 photoreceptor cell pairs within the precluster (Kumar, 2012).

Rough and Senseless participate in a mutual antagonism to specify the cell fate of the equivalence group as either the R8 photoreceptor or R2/5 photoreceptor pair (Figure 8). Rough (Ro) inhibits expression of *senseless* (*sens*), a gene which encodes the Senseless transcription factor necessary for the activation of *ato*. *sens* expression is active within the presumptive R8 photoreceptor, where it inhibits expression of *rough* and promotes expression of *ato*. The cell of the equivalence group which expresses both *ato* and *sens* differentiates into the R8 photoreceptor cell, and cells which express *rough* are directed into the R2/5 photoreceptor fate (Kumar, 2012).

Proceeding specification, the R8 photoreceptor secretes the protein Spitz (Spi). This ligand is received by the EGF receptor (Egfr) of the neighboring equivalence group cells, finalizing R2/5 specification (Kumar, 2012).

The next photoreceptors to be recruited to complete the precluster are the R3/4 photoreceptor cell pair. Four factors are involved in this recruitment and specification; the *seven-up* (*svp*) gene, the *pipsqueak* (*psq*) gene, Frizzled, and Notch (Kumar, 2012).

The Svp protein is distributed in the R3/4 and R1/6 photoreceptor cell pairs. It is genetically upstream of the Egfr pathway and prevents these photoreceptor cell pairs from adopting an inner photoreceptor cell fate. *psq* encodes a transcription factor expressed within the R3/4 photoreceptor pair and is the second step in specifying R3/4 fate. Wingless signals from the morphogenetic furrow are received by the Frizzled receptor of the presumptive R3 and activate expression of Delta within this cell. Delta-Notch signaling then specifies the R4 photoreceptor fate in the neighboring cell. This completes the formation of the ommatidia precluster. R8, R2/5, and R3/4 photoreceptor cells all arise from the cells of the rosette clusters. The last photoreceptor cells to join the precluster, R1, R6, and R7, arise from the daughter cells of the second mitotic division induced by the morphogenetic furrow (Kumar, 2012).

The R1/6 pair is recruited by Egfr signaling and specified by the products of the *Bar* locus, a series of genes that encode a pair of homeobox transcription factors. These proteins are found exclusively within the R1/6 pair (Kumar, 2012). Upon differentiation, the R1/6 photoreceptor cells express Delta, which is significant for the differentiation of R7. The gene *sevenless* (*sev*) encodes a receptor tyrosine kinase expressed in the R7 and the R3/4 photoreceptor cells (as well as four cone cells). However, the Ro and Svp proteins in the R3/4 photoreceptor cells repress the

Sevenless pathway, making it active only in the R7 photoreceptor. This pathway is activated 9-10 rows behind the morphogenetic furrow, and at this point the other photoreceptor cells have differentiated. R8 expresses the membrane-bound protein Bride of sevenless (boss). A combination of Delta-Notch signaling between the presumptive R7 photoreceptor cell and the R1/6 photoreceptor cell pair in addition to Boss-Sevenless signaling between the presumptive R7 and R8 photoreceptor cells determine the fate of this cell (Kumar, 2012). Upon differentiation of R7, all of the photoreceptor cells of the ommatidia cluster have been determined, specified, and differentiated.

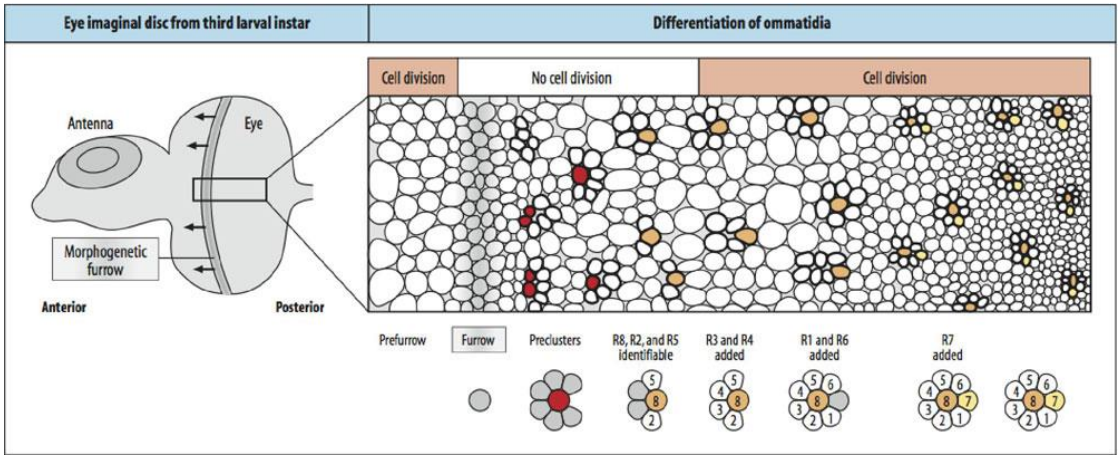

Figure 7. **Progression of the morphogenetic furrow from the posterior compartment of the eye disc drives photoreceptor differentiation.** Photoreceptor differentiation and ommatidial cluster formation occurs during the third larval instar stage. The morphogenetic furrow forms in the posterior compartment of the eye disc and traverses anteriorly, and the photoreceptor cells differentiate in a defined sequence behind the furrow. This developmental cascade is initiated by the formation of R8 and concludes with the differentiation of R7 (Figure adapted from Staveley, B.E, 2014).

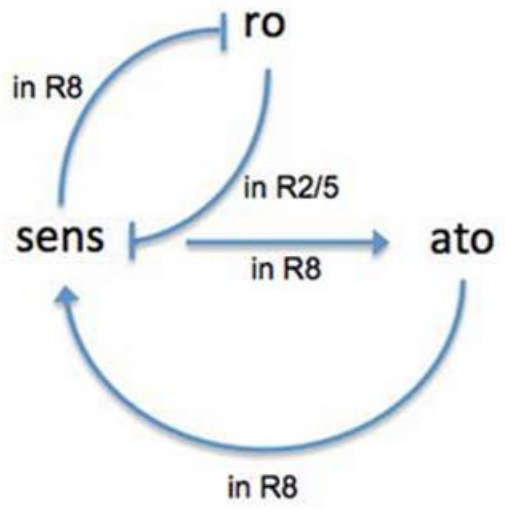

Figure 8. ***ro, sens,* and *ato* genes regulatory circuit.** Rough and Senseless engage in a regulatory network to direct the differentiation of the equivalence group cells to either the R8 or R2/5 photoreceptor cell fate (Figure adopted from Kumar, 2012).

1.4 Greater Initiative

Research being conducted on these two mutants is part of a greater initiative aimed towards gaining a further understanding of the roles of cellular components in Wg and Hh signaling pathways. Because these two pathways are required for numerous phases of *Drosophila* development as well as for adult homeostasis, conducting experiments on various mutants that show phenotypes consistent with loss of Wg or Hh signaling and examining their effects on essential cellular components may aid in the discovery of key mechanisms regulating cell signaling. Furthermore, research on these intronic point mutations may elucidate a novel form of genetic regulation. The goal of these experiments is to identify how the 8J16 and 9E6 intronic point mutations cause their various phenotypes including cold-sensitivity, an embryonic lawn of denticle cuticle, and neurodegeneration. Because of the disrupted

involvement of autophagy, Wg signaling, and Hh signaling in diseases such as cancer, elucidating the interconnected role of these processes could reveal new pharmaceutical targets for treatments or cures (Maiese *et al.*, 2012).

1.5 Specific Aims

The 8J16 and 9E6 intronic point mutations are both in genomic regions that should not have an effect on transcriptional processing as predicted by bioinformatics analysis. However, both mutations yield various phenotypes including cold-sensitivity, a homozygous embryonic lawn of denticle cuticle, neurodegeneration, and deletion-heterozygous late larval/early pupal lethality. The goal of this research is to elucidate the molecular mechanism behind these phenotypes. The specific aims of this research are as follows:

Specific aim 1: Determine if 8J16 and 9E6 mutations result in a splicing defect of the *atg18a* mRNA through RT-PCR experimentation.

Specific aim 2: Examine the molecular nature of the elevated temperature rescue phenotype with qRT-PCR analysis.

Specific aim 3: Analyze the rough eye phenotype in larval imaginal eye discs homozygous for *atg18a* mutant alleles using the FLP-FRT recombination system and subsequent immunofluorescence of neuronal markers.

Specific aim 4: Monitor the effects of the *atg18a* mutations on autophagy using the larval fat body as a model. FLP-FRT recombination system will be utilized to generate mosaicism. LysoTracker® probe will be used to assay the effects.

Specific aim 5: Conduct a rescue experiment utilizing a cDNA *atg18a* transgene in an *atg18a* mutant background to prove that these mutations cause a disruption to Atg18a function and can be rescued with a wildtype copy of the gene.

Chapter 2

MATERIALS AND METHODS

2.1 General *Drosophila* Protocols

Drosophila stocks and crosses were maintained at 25ºC in either vials or bottles containing a standard food media (agar, yeast, sugar, and cornmeal) covered with Carolina™ Blue Food. Once a week, the adult flies would be transferred into fresh vials or bottles. The exception to this would be during stock expansion or maintenance of experimental crosses, in which case flipping would occur every three/four days. Adults would be anesthetized with CO_2 when observations, virgin collection, or male collection needed to be done.

2.2 RNA Isolation

In order to determine the effect of the *atg18a* mutations on transcriptional processing, RNA was isolated from pupae of the genotype $atg18a^{(8J16,\ 9E6,\ or\ P)}/\Delta DF4408$ or $w^{1118}/\Delta DF4408$ using the Total RNA Isolation kit and user manual protocol from Macherey-Nagel's NucleoSpin® RNA II (reference number 740955.50). To ensure that the lab bench was RNase free, all surfaces that would be in contact with the sample were treated with Ambion RNase Zap® (cat.# AM9780). The deletion-heterozygote genotype of the pupa ensured that *atg18a* transcript isolated was coded by the mutant gene ($atg18a^{8J16,\ 9E6,\ or\ P}$). Isolation was conducted with approximately 20 pupae at a time. Extract purity (260/280 of around two for RNA) and concentration (measured in ng/µl) was determined using a Nanodrop. Samples

were distributed into 15 µl aliquots and placed into either the -20°C freezer to await experimentation or the -80°C freezer for long-term storage.

2.3 Polymerase Chain Reaction (PCR)

Following isolation, PCR was conducted on the RNA extract to ensure that the sample was absent of genomic DNA. The logic behind this was that pure RNA samples should be deficient of genomic DNA, and if this was the case there should be no PCR products present. Genomic DNA previously isolated by Erica Boetefuer was used as a positive control. Promega's GoTaq® Hot Start Green Master Mix products and protocol were followed for the experiment. Often a master mix was created with the standard *Taq* Reaction Buffer, the dNTPs, and *Taq* DNA polymerase. Distilled, RNase-free water was first added to sterile PCR tubes on ice, followed by 5 µM each of the appropriate primers (see Appendix A), then 250ng of the RNA sample (volume variable depending on concentration of extract), and proceeded by the master mix to a total volume of 20 µl/tube. The filled PCR tubes were immediately placed into a thermocycler pre-programmed to follow the Promega's GoTaq® Hot Start Green Master Mix protocol: Initial hot start at 94°C for 30 seconds, 30 cycles of 94°C for 15 seconds to denature, 58°C for 30 seconds to anneal the primers, and 68°C for 1.5 minutes to extend the reaction products. The protocol concluded with a final extension at 68°C for 5 minutes, at which point the thermocycler would hold the samples at 4°C until removed.

2.3.1 Agarose Gel Electrophoresis

PCR and RT-PCR products were visualized utilizing agarose gel electrophoresis. For all experiments, a 1% agarose gel was created with Genetic

Analysis Grade Agarose from Fisher Scientific and 1X TAE (see Appendix B). The size of the gel used was variable depending on the number of PCR products to be visualized. Smaller gels required 25 µl, and larger gels required 40 µl. Gels were created in a flask with the appropriate mass of agarose mixed with the appropriate volume of 1X TAE to generate a 1% concentrated gel. The mass of the flask and its contents were measured with a scale before microwaving at 50% power in 20-second intervals. The flask, now containing liquid gel, was then measured for its mass again to ensure that the 1X TAE did not evaporate. If there was a change in mass between the pre- and post-microwave measurements, the difference in water was added and the flask was mixed. Once cooled, the liquid gel was poured into the appropriate gel mold. Upon solidification, the gel was placed into the electrophoresis tank and submerged in 1X TAE. Samples were loaded into the appropriate well, and the electrophoresis was programmed to run for 20 minutes at 100V. To visualize the resolved PCR products, the gel was then transferred into a plastic container and submerged in a diluted ethidium bromide solution for 10 minutes (see Appendix B). The stained gel was rinsed in distilled water for 15 minutes to remove excess ethidium bromide and remove background. Visualization was conducted under a UV light and electronic images were captured using a camera connected to the lab's computer.

2.4 Reverse Transcription Polymerase Chain Reaction (RT-PCR)

RT-PCR analysis was conducted in order to visualize the transcriptional processing of the *atg18a* mRNA in the mutants. Bench areas used for this experiment were maintained RNase free with Ambion RNase Zap® (cat.# AM9780). The primers utilized in this experiment were designed to span intron-exon boundaries of *atg18a*, and calculations were made to determine if the RT-PCR products were indicative of a

properly or improperly spliced *atg18a* transcript (see Appendix A). Three of the five primer pairs were designed for intron-exon boundaries, the fourth was designed as an internal exon control, and the fifth and final primer pair was designed as a positive control for a gene that should always be present (*actin5c*). These experiments were conducted with the Invitrogen product SuperScript® One-Step RT-PCR with Platinum® *Taq* Polymerase and the protocol that came with it. Each sterile PCR tube contained 250 ng of RNA extract (volume was variable depending on concentration of the extract), 5 μM each of the appropriate forward and reverse primers, 1 μl RT/Platinum *Taq* mix, 12.5 μl of the 2x Reaction Mix, and the appropriate amount of distilled water to bring the final volume to 25 μl. The tubes were prepared on ice and placed into a thermocycler pre-programmed to follow the reaction protocol: one cycle at 50°C for 30 minutes, one cycle at 94°C for 2 minutes, 40 cycles of 94°C for 15 seconds, 58°C for 30 seconds, and 72°C for 3 minutes, and one final cycle at 72°C for 5 minutes. The cycler then held the samples at 4°C until retrieval. Visualization by gel electrophoresis was conducted as detailed in 2.3.1.

2.5 Complementary DNA (cDNA) Production

A reagent requirement for qRT-PCR analysis is a cDNA template. Because mutant *atg18a* transcript was to be analyzed with qRT-PCR, cDNA conversation had to be conducted. The RNA extract was utilized as a template to generate cDNA using Bio-Rad's iScript™ cDNA Synthesis kit (catalog # 170-8891). This reaction took place in sterile PCR tubes prepared on ice with 500 ng of total RNA per tube. Each tube additionally contained 4 μl 5x iScript™ mix, 1 μl iScript™ reverse transcriptase, and a differential volume of distilled, RNase free water to a total volume of 20 μl. A thermocycler was pre-programmed to follow the protocol: 5 minutes at 25°C, 30

minutes at 42°C, and finally 5 minutes at 85°C. The cycler maintained samples at 4°C until removed.

2.6 Quantitative Real Time Polymerase Chain Reaction (qRT-PCR)

qRT-PCR analysis was conducted to determine the fold-change of *atg18a* transcript in the deletion-mutant heterozygote RNA extracts relative to wildtype (w^{1118}) RNA extracts. The purpose of this experiment was to determine the molecular basis of the cold sensitive phenotype and the rescue phenotype observed when the deletion-mutant heterozygotes were reared at an elevated temperature. To conduct the experiment, the materials and protocol of QIAGEN's QuantiFast SYBR® Green PCR Kit was utilized. qRT-PCR was conducted in a 96 well plate in which each primer pair reaction was run in triplicate (see Appendix C for primer pairs and well organization). Each well used in the experiment contained 50 ng of cDNA template. To maintain fidelity and organization of the well plate, three master mixes were made with the primer pairs, distilled, RNase-free water, and the reaction mixture provided. The PCR machine was set to cycle through the following protocol: 50°C for 2 minutes, 95.0°C for 5:15 minutes, 60°C for minutes, and 40 cycles of 95°C for 15 seconds (denaturation), 60.0°C for 1 minute (annealing), 95.0°C for 15 seconds, and finally 60.0°C for 15 seconds. Raw data generated was analyzed in Excel.

2.6.1 Data Analysis of qRT-PCR Data

Excel was used to complete all computations of the qRT-PCR data. The spreadsheet was set to follow the statistical analysis provided by Volume 2 of "Current Protocols in Molecular Biology," page 15.8.9.

2.7 Eye Tissue-Specific Mitotic Recombination

Among the genetic tools and manipulations available for use in the *Drosophila melanogaster* genetic model is the FLP-FRT methodology. It is utilized to generate homozygous mutant clones in an otherwise heterozygous background. Endogenous to yeast, the site-specific recombinase flippase (FLP) is able to recognize flippase recognition target (FRT) sites and induce recombination between these sites. FRT sites have been recombined onto each arm of *Drosophila* chromosomes (Theodosiou and Xu, 1998). This allows for mitotic recombination to occur between homologous chromosomes (Figure 9).

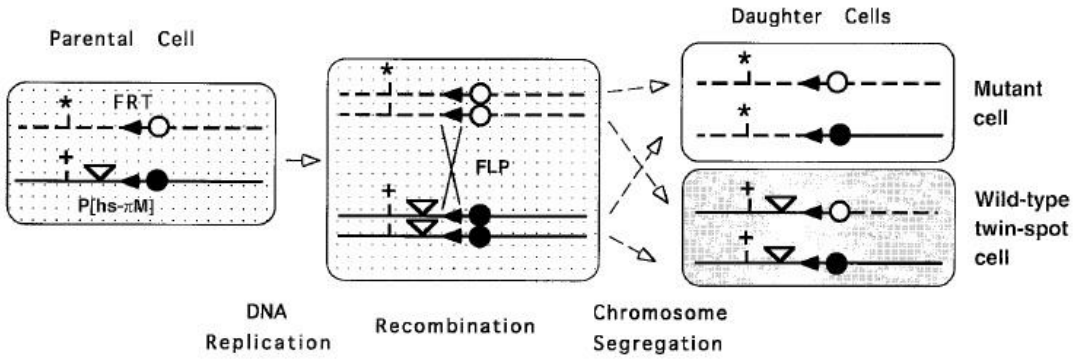

Figure 9. **FLP/FRT recombination induces mitotic recombination between non-sister homologous chromosomes.** Following S phase of the cell cycle, FLP induces mitotic non-sister homologous recombination between FRT sequences (black arrow on chromosome). This process results in the generation of a homozygous mutant cell in an otherwise heterozygous organism (Figure adapted from Theodosiou and Xu, 1998).

The *atg18a* mutations give rise to a neurodegenerative phenotype. Because the adult eye is not necessary for viability of the organism, the *Drosophila* eye was used

as a model to study the effects of these mutants on neuronal development. The genotype for this experiment was: *w/w; eyGal4:UASFLP/+; atg18a*$^{8J16,9E6,\ or\ P\ FRT2A}$*/gmr-hid*^{FRT2A}. The *eyeless (ey)* promoter is endogenous to the *Drosophila* eye, and it is active during the first larval instar. Gal4 can bind to an upstream-activation sequence (UAS) to enhance and activate expression of the downstream gene (FLP in this case). Because the *ey* promoter is active only within the eye, Gal4 was expressed only within this tissue to drive downstream expression of FLP. Thus, mitotic recombination was induced within developing eye tissue exclusively. Following mitosis, two possible daughter cells that could be formed would be homozygous for the *atg18a* mutation or *gmr-hid*. Because it is a dominant-functioning gene, *gmr-hid* induces apoptosis when heterozygous or homozygous. The only cells remaining within the eye would be homozygous mutant for *atg18a*, creating an ideal model for study.

2.7.1 Imaging of the Adult Eye Phenotype

Because *Drosophila* with the *w/w; eyGal4:UASFLP/+; atg18a*$^{8J16,9E6,\ or\ P\ FRT2A}$*/gmr-hid*^{FRT2A} phenotype are heterozygous for the *atg18a* mutations, they can survive through development to adulthood. By observing the adult homozygous mutant eye, the adult neurodegenerative phenotype could be characterized. Several males and females of each mutation (9E6, 8J16, and P) were isolated and placed into sterile microcentrifuge tubes. These tubes were placed in the -20°C freezer to kill the flies. Following this treatment, the flies were placed under the Nikon SMZ800 microscope and images were captured. CO_2 treatment was not sufficient to anesthetize the flies for imaging.

2.7.2 Larval Imaginal Eye-Antennal Disc Dissection

To study the effects of the *atg18a* mutations on neuronal development, imaginal eye-antennal discs were dissected from third instar larvae of the genotype *w/w; eyGal4:UASFLP/+; atg18a*$^{8J16,9E6,\ or\ P\ FRT2A}$*/gmr-hid*^{FRT2A}. These larvae could be distinguished from those of other genotypes due to their wildtype larval shape relative to the larvae with a tubby phenotype. Primary dissection occurred in 1X PBS under the dissecting microscope (see Appendix B). The mouth parts of the larva were tugged to remove the brain and the connected imaginal eye-antennal disc. This tissue was fixed in 1x PBS with 4% formaldehyde for 20 minutes at room temperature on a rocker. The 4% formaldehyde solution was then removed, and the structures were rinsed and washed for five minutes four times each in PBT (see Appendix B). Following the rinse and wash cycle, the structures were blocked with PBT with 5% Normal Horse Serum (PBTN) for 30 minutes. The structures were then incubated in primary antibody diluted in PBTN on a rocker for two hours at room temperature or overnight at 4°C. Primary antibodies utilized in this experiment were targeted against either a neuronal marker or the apoptotic marker cleaved-caspase 3 (see Appendix D). Proceeding primary antibody treatment, the structures underwent another four rounds of rinsing and washing with PBT. They were then incubated in secondary antibody in PBTN for one hour at room temperature. Secondary dissection was then conducted under the dissecting microscope in PBT to isolate the imaginal eye disc from the eye-antennal structure. Dissected eye discs were mounted on a microscope slide in a 70% glycerol-PBS solution, covered with a Fisherbrand® Micrscope Cover Glass, and sealed with nail polish. Slides were visualized and images captured with the Zeiss LSM780 confocal microscope. Images were processed using ImageJ software.

2.8 Positively marked clones for Monitoring of Autophagy in the Larval Fat Body

In *Drosophila*, the larval fat body is a model tissue known to be studied for autophagy (Nagy *et al.*, 2015). Thus, to determine the effect of the *atg18a* mutations on autophagy, FLP-FRT recombination techniques were utilized to generate mosaicism in the fat body for side-by-side comparison of homozygous mutant cells with heterozygous mutant cells. It should be noted that the wildtype *atg18a* is dominant to the mutant *atg18a* genes, and therefore these heterozygous mutant cells are metabolically representative of wildtype cells. The genotype of the larva studied for this purpose was *hsFLP, tubGal4, UASgfp*^{nls}*/ hsFLP, tubGal4, UASgfp*^{nls}*; tubGal80*$^{FRT\ 2A}$*/atg18a*$^{8J16\ or\ 9E6\ FRT\ 2A}$. The ubiquitously active *tub* promoter expresses the downstream gene throughout the entire *Drosophila* body (*gal80* and *gal4* in this genotype). Gal80 is a repressor of Gal4; if Gal80 is present, then genes downstream of a UAS (*gfp*^{nls} in this genotype) cannot be expressed. Three days after making the cross to generate this genotype, the adults were flipped into a new vial, and the vial containing the embryos was heat-shocked at 37°C for one hour. This activated the heat-shock promoter and expression of FLP, which then induced mitotic non-sister homologous recombination between 3rd chromosomes containing *tubGal80*$^{FRT\ 2A}$ and *atg18a*$^{8J16\ or\ 9E6\ FRT\ 2A}$. Following chromosomal segregation and cellular division, one resultant daughter cell would be homozygous for the *atg18a* mutation and the other would be homozygous for *tubGal80*$^{FRT\ 2A}$. In the absence of Gal80, Gal4 is able to bind to the UAS to drive gfp^{nls} expression. Because the only cells deficient of Gal80 would be homozygous *atg18a* mutants, the presence of gfp in the nucleus of these cells marked *atg18a*$^{8J16\ or\ 9E6}$ homozygous mutant cells. Using this methodology,

mosaic analysis could be performed on homozygous mutant cells in a heterozygous mutant background.

2.8.1 Larval Fat Body Dissection and Lysotracker® Treatment

In order to determine the effects of the *atg18a* mutants on autophagy, the fat body was utilized as a model. For this experiment, the reagent Invitrogen™ Lysotracker® Red DND-99 (catalog number L-7528) was used. Because the fat body is an unstable structure outside of the larva, the following procedure previously developed by Erica Boetefuer had to be followed with swiftness. Larvae utilized for this experiment were starved to induce autophagy, and fed larvae were used as a control. Larvae were placed in a 20% sucrose solution for 3.5 hours to cause starvation. The larva dissection procedure went as follows: early 3rd instar larvae were collected from the vials in which they grew and washed in water to clear them of media particulate. They were then placed in a dissection chamber with 1X PBS and bisected to expose the fat to solution. The bisected larvae were placed into a microcentrifuge tube filled with a Lysotracker® solution (0.5 µl Lysotracker® in 5000 µl 1X PBS) for three minutes. Proceeding treatment, the bisected larvae were placed back in the dissection chamber to isolate the fat body, which was then placed into a microcentrifuge tube containing 4% formaldehyde in 1X PBS for a 3 minute fixation. Immediately after this, the fat body was mounted in 1X PBS on a slide, covered with a Fisherbrand® Micrscope Cover Glass, and sealed with nail polish. Due to the unstable nature of the fat body, images had to be captured and recorded as soon as possible. Images were initially taken with a fluorescent Zeiss Auxiophot microscope but eventually taken with a Zeiss LSM780 confocal microscope.

2.9 Generation of the Rescue Experiment

To determine that the phenotypes observed in 9E6 and 8J16 are the result of a disruption to the *atg18a* gene product, a rescue experiment was designed that would introduce a cDNA transgenic insertion of the wildtype *atg18a* in a homozygous mutant background. Thanks to the generosity of Dr. Juhasz, Dr. Selva's laboratory was able to acquire transgenic *Drosophila* from his laboratory harboring a *UASmcherry-atg18a* gene on the second chromosome. Dr. Gabor's experimentation with this transgene construct suggests that the chimeric mcherry-atg18a protein functions properly and should be able to give a rescue phenotype in a mutant background (Nagy *et al.*, 2014). While the experiment has not yet been completed, the plans to establish the genetics have been detailed (see Appendix E).

Chapter 3

RESULTS

3.1 Transcriptional Processing is not Disrupted in *atg18a* Mutants

Because the *atg18a* mutations studied are all intronic, point mutations, it was hypothesized that 9E6 and 8J16 cause a phenotype as a result of faulty transcriptional processing of the *atg18a* mRNA. RT-PCR analysis using primers that spanned intron-exon boundaries was conducted to investigate if this was the case (see Appendix A). Gel electrophoresis and ethidium bromide staining of the RT-PCR products revealed that splicing of the 8J16 and 9E6 mRNA transcripts is identical to that of wildtype (Figure 10). Presence of *actin5c* was included as a positive, external control, for it should be present in all RNA extracts.

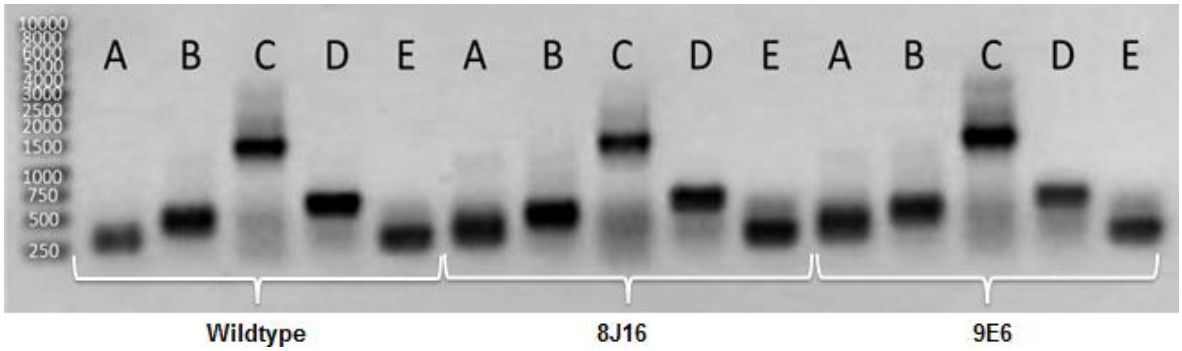

Figure 10. **Transcriptional processing of the *atg18a* mRNA is not defective in deletion-heterozygote mutants harboring the 9E6 or 8J16 mutation.** 1 kb DNA ladder was used to indicate relative molecular weights of gel bands. Refer to Appendix A for primer pairs utilized. Calculations were made to determine if the molecular weight of the primer pair bands were indicative of a properly or improperly spliced message. Both 8J16 and 9E6 show identical bands as the wildtype *atg18a* mRNA, and this suggests that the mutations do not cause improper transcriptional processing of the *atg18a* mRNA.

3.2 Relative *atg18a* Transcriptional Fold Differences Does not Explain Cold Sensitive Phenotype

To investigate the cold sensitive and temperature permissive phenotypes of deletion-heterozygote in *Drosophila* harboring the 8J16 and 9E6 mutations, qRT-PCR was conducted on total RNA extracted from pupae of the genotypes $w^{1118}/\Delta DF4408$, $9E6^{FRT\ 2A}/\Delta DF4408$, $8J16^{FRT\ 2A}/\Delta DF4408$, and $atg18a^{P}/\Delta DF4408$ reared at both 25°C and 29°C. The rationale for this experiment was twofold. First, the 29°C rescue phenotype for 8J16 and 9E6 was possibly due to stabilization or increased expression of *atg18a* mRNA at the elevated temperature. Second, the *atg18a* mRNA from 8J16 and 9E6 deletion heterozygotes would be reduced relative to wildtype at 25 °C and to a lesser extent at 29 °C. This would have been predicted to result in an increase of the *atg18a* mRNA in flies of the same genotype reared at 29°C relative to those reared at 25°C, and a higher level of mRNA in the wildtype relative to the mutants at the same

temperature. Although these experiments were repeated several times, the statistical analysis of the data did not provide statistically significant conclusions for either hypothesis due to variability of the results (data not shown; see Appendix F). A consistency that was observed; however, was the decrease in the *atg18a* transcript in wildtype *Drosophila melanogaster*. Increased autophagic activity has been found to follow heat shock in order to clear the cytoplasm of damaged organelles and misfolded proteins, making this negative fold change a peculiar observation (Swanlund et al., 2008).

3.3 Photoreceptor Nerve Cells Homozygous for *atg18a* Mutations Succumb to Apoptosis (Exception: R7 and R8 are Refractory)

Investigation of the neurodegenerative phenotype displayed by 8J16 and 9E6 mutants was done by observing homozygous mutant 3rd instar larva imaginal eye discs utilizing immunofluorescence and confocal microscopy. Antibodies were targeted against neuronal markers and cleaved-caspase 3 (see Appendix D). Analysis of the apoptotic marker, cleaved-caspase 3 (Figure 11, green), the R7 specific marker Prospero (Figure 11, red), and the pan neuronal marker, ELAV (Figure 11, blue), revealed that *atg18a*^{8J16} and *atg18a*^{9E6} mutant photoreceptors are succumbing to apoptosis during development of the eye disc. This is evident near the posterior end of the eye disc, where it appears that photoreceptors which have differentiated earliest are being lost and at the morphogenetic furrow (Figure 11, green arrows). Interestingly, R7 photoreceptors are refractory to this apoptotic event. This is indicated by the presence of Prospero-expressing R7 cells (Figure 11, red) among the few photoreceptors left within ommatidial clusters near the posterior, where few ELAV positive photoreceptors remain (Figure 11, blue). Figure 12 shows that Senseless

expressing R8 photoreceptor cells (blue) are also refractory to the apoptotic event, as R8 cells are among the only remaining photoreceptors within the ommatidial clusters in the posterior where few ELAV positive photoreceptors remain (Figure 12, green).

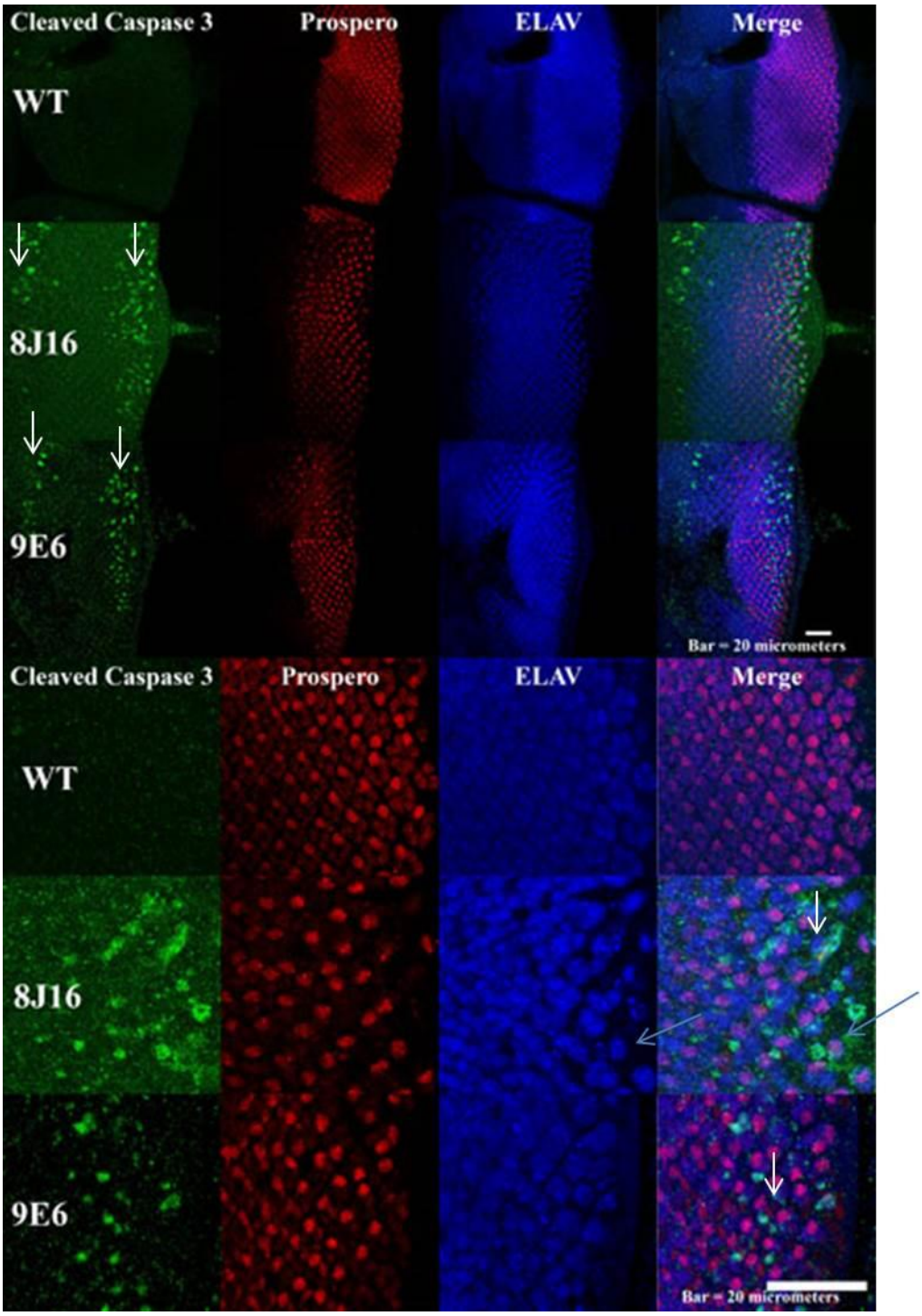
Cleaved Caspase 3
Prospero
ELAV
Merge
WT
8J16
9E6
Bar = 20 micrometers
Cleaved Caspase 3
Prospero
ELAV
Merge
WT
8J16
9E6
Bar = 20 micrometers

Figure 11. **Nerve cells homozygous for 8J16 or 9E6 succumb to apoptosis during development, and the R7 photoreceptor cell is refractory to this event.** Expression of cleaved caspase 3 (green), an apoptotic marker, Prospero (red), a homeobox protein and neuronal marker for the R7, and ELAV (blue), a pan-neuronal marker, in eye imaginal discs from 3rd instar larvae. The presence of cleaved caspase 3 in the mutant eye indicates that the photoreceptors are succumbing to apoptosis. Bottom panels showing high magnification on ELAV expression reveals that many clusters have fewer photoreceptors, though Prospero is still expressed. Cells expressing cleaved caspase 3 are Prospero negative, indicating that R7 is refractory to apoptosis and survive longer in both *atg18a*^{8J16} and *atg18a*^{9E6}.

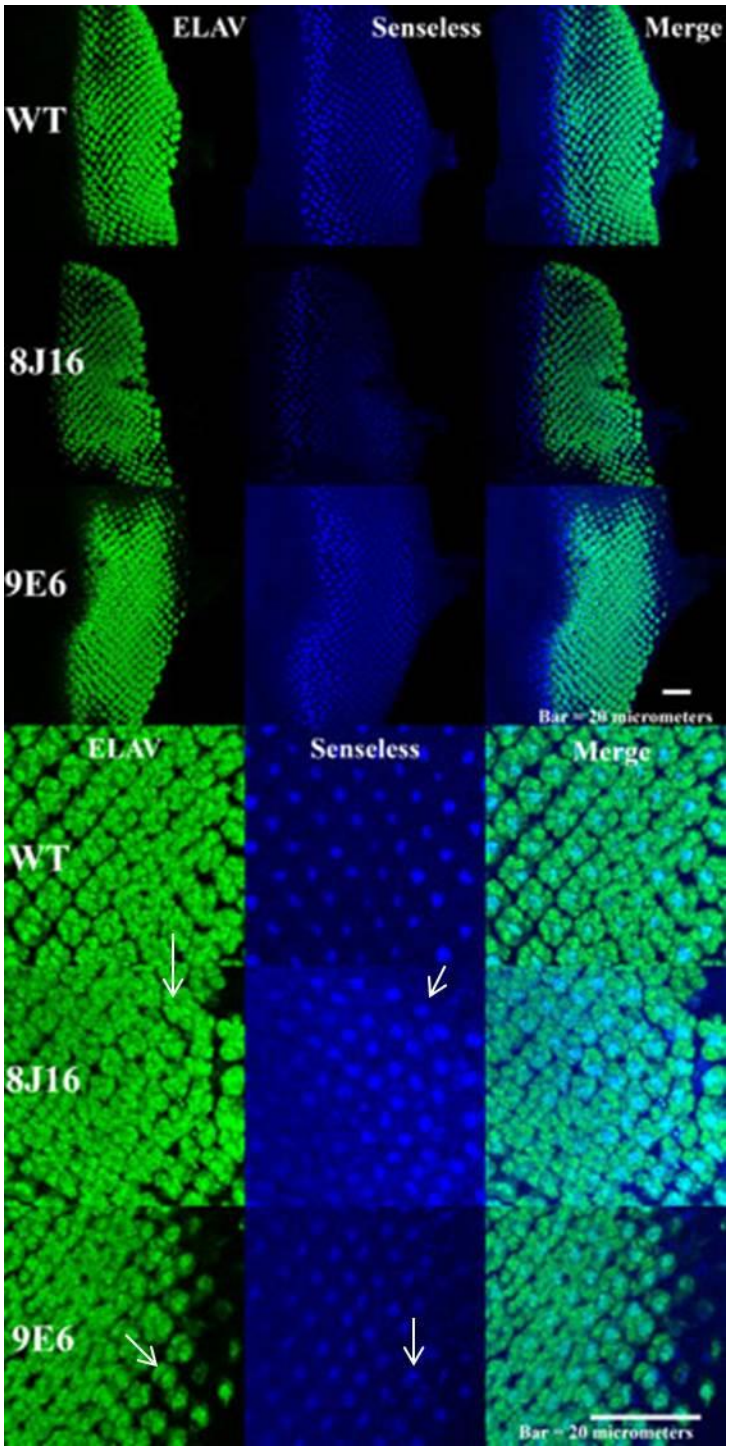
ELAV
Senseless
Merge
WT
8J16
9E6
Bar = 20 micrometers
ELAV
Senseless
Merge
WT
8J16
9E6
Bar = 20 micrometers

Figure 12. **R8 photoreceptor cell is refractory to the nerve cell apoptotic phenotype observed in *Drosophila* harboring the 8J16 or 9E6 mutations.** Expression of ELAV (green) and Senseless (blue), a zinc finger transcription factor and marker for R8 photoreceptors, in eye imaginal discs from 3rd instar larvae. R8 develops properly in both $atg18^{8J16}$ and $atg18^{9E6}$, and it is refractory to apoptosis as suggested by the presence of Senseless expressing photoreceptors in ommatidia with fewer than the full complement of photoreceptors (white arrow). Bottom panel is higher magnification.

3.4 *atg18a* Mutations do not Disrupt Autophagy in Cells of the Fat Body

RT-PCR experimentation revealed that the 8J16 and 9E6 mutations do not seem to cause gross errors in transcriptional processing of the *atg18a* mRNA. However, these mutations still cause several severe phenotypes. It was hypothesized that these phenotypes are a result of an Atg18a protein that does not function properly, which would be expected to disrupt autophagic activity within the fat body of larvae harboring these homozygous mutations. As described in 2.8, the genotype of the assayed larvae allowed for mosaic analysis of homozygous *atg18a* mutant cells adjacent to those that carry one wildtype copy of the gene. Lysotracker® treatment and subsequent fluorescent imaging revealed that the homozygous mutant cells are forming numerous lysosomal punctae under starvation conditions, a phenotype generally associated with autophagic activity (Figures 13 and 14; Nagy *et al.*, 2015).

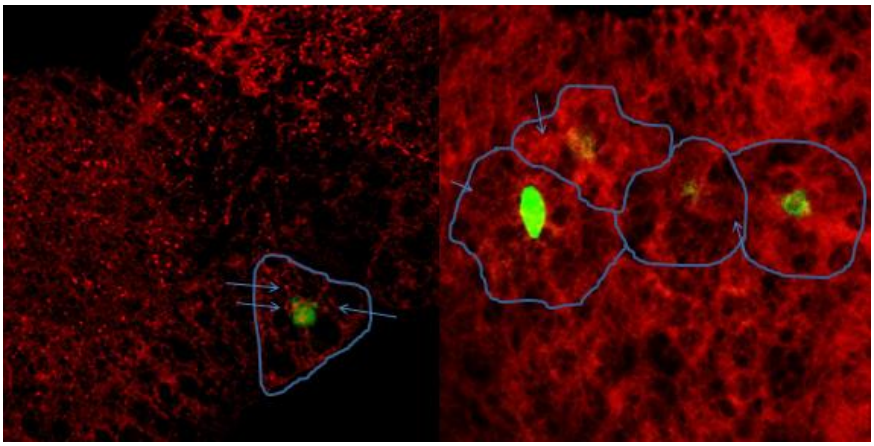

Figure 13. **Lysosomal punctae (blue arrow) can be observed in both starved (left) and fed (right) homozygous *atg18a*^{8J16} larval fat body cells**. The presence of nuclear green fluorescent protein (GFP) acts as a marker for homozygous mutant clone cells in an otherwise heterozygous background. Lysosomal punctae within these cells suggests that autophagy is not disrupted by the 8J16 mutation. Note the increase in punctae concentration in the starved cells as compared to the fed cells, as starvation increases autophagy.

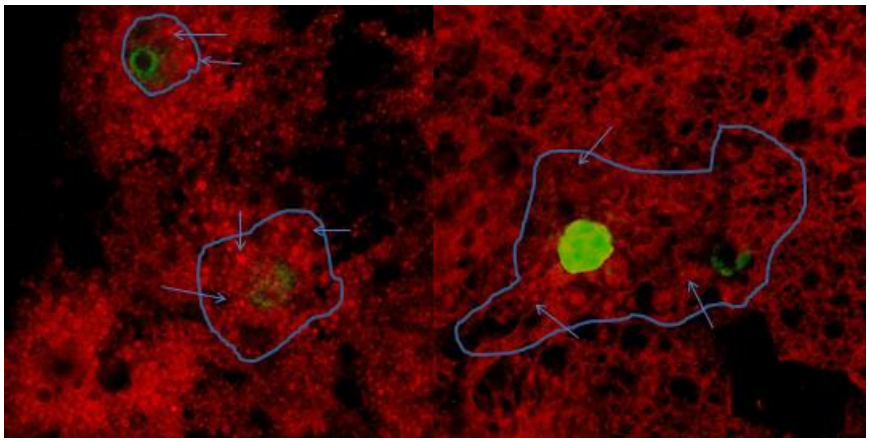

Figure 14. **Lysosomal punctae (blue arrow) can be observed in both starved (left) and fed (right) homozygous *atg18a*^{9E6} larval fat body cells**. The presence of nuclear GFP acts as a marker for homozygous mutant clone cells in an otherwise heterozygous background. Lysosomal punctae within these cells suggests that autophagy is not disrupted by the 9E6 mutation. Note the increase in punctae concentration in the starved cells as compared to the fed cells.

Chapter 4

DISCUSSION

4.1 Transcriptional Processing of the *atg18a* mRNA

My initial hypothesis was that the phenotypes observed in the *atg18a* mutants were a consequence of faulty processing of the *atg18a* transcript as both 9E6 and 8J16 point mutations are located within introns of the *atg18a* locus. I hypothesized that improper splicing of the *atg18a* message would cause improper encoding of the Atg18a protein downstream of the defect, resulting in production of a nonfunctional protein product. RT-PCR experimentation revealed data contrary to my hypothesis, as the *atg18a* mRNA extracted from 8J16 and 9E6 mutants has the same molecular weight as that of wildtype *atg18a* mRNA. This suggests the message is being spliced correctly in these backgrounds. However, due to the nature of the primers utilized in the RT-PCR experimentation, the data gathered can only indicate if the introns have been properly spliced out of the transcript. There is a possibility that the mutations are inducing an alternative splicing event which results in the generation of a transcript which cannot properly code for the Atg18a protein. Future experimentation is required to determine if this is the case. It should be noted that the mutant transcripts have not been sequenced. This is a potential experiment that could be conducted in the future to see if the point mutations are causing small changes during transcriptional processing which could not be resolved by gel electrophoresis.

The cold sensitive and temperature permissive phenotypes of the *atg18a* mutants studied was hypothesized to be the result of either increased expression of the *atg18a* transcript or destabilization of an improperly coded, partial dominant-negative

functioning Atg18a protein at the higher temperature. This was investigated with qRT-PCR analysis. Data acquired was not statistically significant and contradicted the data found previously by those who performed similar experiments for this project before me. The variable nature of these data indicate fold changes of the *atg18a* transcript found in these experiments could not be considered reliable results from which any concrete conclusions can be drawn.

4.2 Neurodegenerative Phenotype

Before I began work on this project, it was observed that the 8J16 and 9E6 mutant alleles cause neurodegenerative phenotypes in embryos. To further characterize this phenomenon, I studied homozygous mutant neurons in the eye of the fly in an otherwise heterozygous background. Adults of this genotype display a rough eye phenotype, and it was hypothesized that autophagy is required for neuronal maintenance and in its absence neuronal apoptosis ultimately results. This possibility was investigated by immunofluorescence of the mutant imaginal eye discs targeted against cleaved-caspase 3, a marker of apoptosis. These experiments revealed there was indeed a high level apoptotic activity, particularly at both the posterior end of the eye disc where the earliest differentiating photoreceptors reside and the morphogenetic furrow. Excessive apoptosis in these regions was not observed within the wildtype imaginal eye disc, suggesting that it is the result of either the 8J16 or 9E6 homozygous mutations. While the high apoptotic activity within the morphogenetic furrow could indicate that the rough eye phenotype is the result of a smaller number of photoreceptor progenitors, the apoptotic activity in the posterior end of the eye disc suggests that those photoreceptors which differentiate earliest are being lost. It should be noted that examination of Senseless and Prospero expression showed that

photoreceptor cells R8 and R7, respectively, are more refractory to apoptosis, as these photoreceptors predominate near the optic stalk where the photoreceptor cells initiate differentiation. This suggests autophagy is more important for the maintenance of photoreceptors R1, R2, R3 R4, R5 and R6 than R7 and R8. The specific nerve cells succumbing to apoptosis have not been identified, and further experimentation will need to be conducted to draw this conclusion. While the molecular cause of the apoptotic activity found to occur in the R1-R6 photoreceptor cells has not been identified, the function of these cells is to detect motion and presence of light, much like the rods of the human eye. The R7 and R8 photoreceptor cells, which do not apoptose, are responsible for detecting color within the visible and ultraviolet spectra (Takemura et al., 2008). This duality in function and the transduction pathways involved may be correlated to the unusual apoptotic activity observed within the mutants. Additionally, while the involvement of autophagy and apoptosis in neurodegeneration is not molecularly understood, both pathways have been observed in human neurodegenerative diseases (Lionaki *et al*., 2015). This adds significance to the continued study of how the 8J16 and 9E6 alleles give rise to the unusual neuronal apoptotic phenotype observed in the R1-R6 photoreceptor cells.

4.3 Effect of the *atg18a* Mutations on Autophagy

Up to this point in my project's history, while it was determined that the 8J16 and 9E6 alleles disrupt normal embryonic development and cause neurodegeneration in the eye, it was not determined that these alleles cause a disruption to the functionality of the Atg18a protein. Unfortunately, there are no available antibodies against *Drosophila melanogaster* Atg18a, so analysis of the protein is not an option. In order to examine possible autophagy defects caused by these mutations, *atg18a*^{8J16}

and *atg18a*^{9E6} homozygous mutant larval fat body was starved to induce autophagy (larvae were fed in control experiments). Autophagy was investigated by observing the relative quantity of Lysotracker® positive punctae formed in homozygous mutant cells as compared to neighboring cells harboring one wildtype copy of the gene. Lysosomal punctae were observed in the homozygous mutant cells under starved conditions, suggesting 8J16 and 9E6 mutants are able to properly operate the process of autophagy. However, because Lysotracker® stains any vesicle containing lysosomal enzymes and is notoriously difficult to work with due to its innate instability, this experiment did not follow an ideal method for assaying autophagy. Future experiments using additional markers of autophagy should be conducted to draw a strong conclusion of whether or not the 8J16 and 9E6 mutations disrupt autophagy.

4.4 Conclusions

The following conclusions have been drawn from this project regarding the *atg18a* intronic point mutations 8J16 and 9E6:

1. No evidence was obtained indicating 8J16 and 9E6 mutant alleles caused faulty transcriptional processing of the *atg18a* mRNA.
2. Photoreceptor cells homozygous for either the 8J16 or 9E6 allele are dying due to apoptosis (particularly at the morphogenetic furrow and the posterior end of the eye disc). Those photoreceptor cells that differentiate early are being lost in 3rd instar larva and probably through pupal development. Because they are not likely replaced, this yields the adult rough eye phenotype.

3. Though the specific nerve cells succumbing to apoptosis have not been identified, the R7 and R8 photoreceptor cells are refractory to apoptosis as they predominate near the posterior end where photoreceptors differentiate first.
4. Autophagy does not appear to be affected by the 8J16 or 9E6 alleles, though this requires further examination.

4.5 Future Directions

As the observations made throughout researching this project have revealed negative data, much work is to be done to properly identify the molecular basis of the phenotypes caused by the 8J16 and 9E6 mutations. Below are the proposed actions required to progress:

1. Completion of the rescue experiment

Results from the rescue experiment will indicate if the 8J16 and 9E6 alleles cause phenotypes by disrupting proper production of the *atg18a* gene product. If the experiment yields *Drosophila* with a rescue (wildtype) adult eye phenotype, then it can be determined that this is the case. In the event that rescue does not occur then perhaps the molecular mechanism of these intronic mutations' phenotypes is a novel genetic regulatory phenomena not yet understood. Within the introduction, it was mentioned that the core molecular components of autophagy can be involved in processes other than autophagy. If the experiment yields a rescue phenotype and yet autophagy is not found to be disrupted in homozygous tissue, it could be concluded that Atg18a has a molecular role in processes other than autophagy within *Drosophila melanogaster*, and these other processes ultimately affect Wg/Hh signaling, neuronal health/development, and cold sensitivity.

2. Investigate aberrant splicing induced by mutant alleles via sequencing of the *atg18a* transcript or northern blot analysis

While RT-PCR analysis revealed that the molecular weight of the mutants' *atg18a* transcript is identical to that of wildtype, it did not reveal the structure of the transcript. There is a possibility that the mutations are inducing an alternative splicing event which results in the generation of a transcript which cannot properly code for the Atg18a protein. This could be investigated with northern blot analysis utilizing probes specific to each exon of the *atg18a* gene locus. Another investigative alternative would be to sequence the mutant *atg18a* transcripts after gel purifying the RT-PCR products.

3. Repeat qRT-PCR for more data

The qRT-PCR experiment was not conducted more than four times throughout my work on the project. There is a possibility that the reason statistically significant results have not been observed is due to a low sample size. Repetition of the experiment could indicate if this is the case.

4. Continue to investigate the effect of the mutant alleles on autophagy using assays other than Lysotracker®

Lysotracker®, while widely accepted as a reagent for use to assay autophagy, is difficult to work with for two major reasons. Because the reagent marks for lysosomal markers, it is not an autophagy-specific marker. It is utilized in autophagic assays because autophagy increases lysosomal concentration within the cell (Nagy *et al*., 2015). In order to properly indicate if the 8J16 and 9E6 mutations disrupt autophagy, it is proposed that alternative assays be utilized in the future. Two such examples would be to assay for the autophagic markers p62 or LC3. p62 is an

autophagic cargo and accumulates as a result of autophagy (Nagy *et al.*, 2015). Immunofluorescence against p62 can identify if autophagy is disrupted if limited punctae are observed (as compared to wildtype). LC3 also accumulates as a result of autophagy, and immunofluorescence can be utilized to make the same observation (Nagy *et al.*, 2015). The second reason Lysotracker® is difficult to work with is that the reagent is highly labile and unstable.

REFERENCES

Boetefuer, E. (2012). The role of atg18 in signal transduction pathways during Drosophila development.

Feng, Y., He, D., Yao, Z., & Klionsky, D. J. (2014). The machinery of macroautophagy. *Cell Res, 24*(1), 24-41. doi: 10.1038/cr.2013.168

Feng, Y., Yao, Z., & Klionsky, D. J. (2015b). How to control self-digestion: transcriptional, post-transcriptional, and post-translational regulation of autophagy. *Trends Cell Biol*. doi: 10.1016/j.tcb.2015.02.002

Kumar, J. P. (2012). Building an ommatidium one cell at a time. Dev Dyn, 241(1), 136-149. doi: 10.1002/dvdy.23707

Lionaki, E., Markaki, M., Palikaras, K., & Tavernarakis, N. (2015). Mitochondria, autophagy and age-associated neurodegenerative diseases: New insights into a complex interplay. Biochim Biophys Acta. doi: 10.1016/j.bbabio.2015.04.010

Lőrincz, P., Lakatos, Z., Maruzs, T., Szatmári, Z., Kis, V., & Sass, M. (2014). Atg6/UVRAG/Vps34-containing lipid kinase complex is required for receptor downregulation through endolysosomal degradation and epithelial polarity during Drosophila wing development. *Biomed Res Int, 2014*, 851349. doi: 10.1155/2014/851349

Maiese, K., Chong, Z. Z., Shang, Y. C., & Wang, S. (2012). Targeting disease through novel pathways of apoptosis and autophagy. *Expert Opin Ther Targets, 16*(12), 1203-1214. doi: 10.1517/14728222.2012.719499

Nagy, P., Hegedűs, K., Pircs, K., Varga, Á., & Juhász, G. (2014).Different effects of Atg2 and Atg18 mutations on Atg8a and Atg9 trafficking during starvation in Drosophila. FEBS Lett, 588(3), 408-413.

Nagy, P., Varga, Á., Kovács, A. L., Takáts, S., & Juhász, G. (2015). How and why to study autophagy in Drosophila: It's more than just a garbage chute. Methods, 75, 151-161. doi: 10.1016/j.ymeth.2014.11.016

Selva, E. M., & Stronach, B. E. (2007). Germline clone analysis for maternally acting Drosophila hedgehog components. Methods Mol Biol, 397, 129-144. doi: 10.1007/978-1-59745-516-9_11

Staveley, B.E. (2014). Molecular & developmental biology. Retrieved from http://www.mun.ca/biology/desmid/brian/BIOL3530/DB_09/DBNOrgan.html

Swanlund, J. M., Kregel, K. C., & Oberley, T. D. (2008). Autophagy following heat stress: the role of aging and protein nitration. Autophagy, 4(7), 936-939.

Takemura, S. Y., Lu, Z., & Meinertzhagen, I. A. (2008). Synaptic circuits of the Drosophila optic lobe: the input terminals to the medulla. J Comp Neurol, 509(5), 493-513. doi: 10.1002/cne.21757

Theodosiou, N. A., & Xu, T. (1998). Use of FLP/FRT system to study Drosophila development. Methods, 14(4), 355-365. doi: 10.1006/meth.1998.0591

Xie, Z., & Klionsky, D. J. (2007). Autophagosome formation: core machinery and adaptations. Nat Cell Biol, 9(10), 1102-1109.

Appendix A

PRIMERS UTILIZED FOR PCR AND RT-PCR ANALYSIS

Primer	Sequence (5’ to 3’)
1418F	TAAAGCGCTGTGTGTCCATC
2439R	TGCTTTTGTATCGTGGCAAT
2958R	ATGGCATAGTGGTCCTCCAG
129F	TAGTCAACAGCGGTGTCCTG
3187R	AACAGAAACAGCCGACTTGC
938F	GAGAGCTCCTTGGTGGCAATAGT
1509R	GAAGATGTGAACCGTCTCGGTGT
Actin5C 1175F	CTCGCCACTTGCGTTTACAGTAG
Actin5C 2049R	ATGGGGTACTTCAGGGTGAGGATA

PRIMER PAIRS AND EXPECTED MOLECULAR WEIGHTS OF SAMPLES

Expected weight (defective splicing) refers to the molecular weight of the agarose gel band that would be expected of *atg18a* mRNA transcripts which were not processed correctly.

Referenced Letter	**Primer Pair**	**Expected Weight (Spliced)**	**Expected Weight (Defective Splicing)**
A	1418F-2439R	316	1021
B	1418F-2958R	438	1540
C	129F-3187R	1461	3058
D	938F-1509	571	571
E	Actin5C 1175F-Actin5C 2049R	282	875

Appendix B

SOLUTIONS

- **50x Tris, Acetic Acid, EDTA (TAE) Stock Solution:** 242 g Tris Base (MW=121,1), 57.1 mL Glacial Acetic Acid, 100 mL 0.5 M EDTA (mix Tris with stir bar to dissolve in 600 mL of ddH_20, add EDTA and Acetic Acid, bring final volume to 1 L with ddH_20, and store at room temperature). Dilute to working concentration (1X) using diH_20.

- **Ethidium Bromide Solution:** 10 µl ethidium bromide (10 mg/ml) in 200 ml distilled water.

- **1X Phosphate Buffered Saline (PBS):** 10 mM phosphate (pH 7.4), 183 mM NaCl, 27 mM KCl

- **1X Phosphate Buffered Saline with Triton-X 100 (PBT):** 10 mM phosphate (pH 7.4), 138 mM NaCl, 27 mM KCl, 0.1% Triton-X 100, 0.1% BSA

Appendix C

PRIMERS AND PRIMER PAIRS FOR qRT-PCR

Primer	Sequence (5’ to 3’)
160F	AGG GCC GAG GCA GAG GTG TT
287R	TTC GCC CGC ATC CAC ATC GG
938F	CAT CGT TTC GCT GTC GTT TA
1089R	AGT AAC CCA TCC AGT CGT CG
Actin5C 332F	GGC GCA GAG CAA GCG TGG TA
Actin5C 455R	GGGTGCCACACGCTCAT

Pairs (letters refer to well plate):
A: 160F-287R
B: 938F-1089R
C: Actin5C 332F-Actin5C 455R

Template cDNA
1) WT 25°C
2) WT 29°C
3) 9E6 25°C
4) 9E6 29°C
5) 8J16 25°C
6) 8J16 29°C

Well Plate Setup

	1	2	3	4	5	6	7	8	9	10	11	12
A												
B	A1	C1	A2	C2	A3	C3	A4	C4	A5	C5	A6	C6
C	A1	C1	A2	C2	A3	C3	A4	C4	A5	C5	A6	C6
D	A1	C1	A2	C2	A3	C3	A4	C4	A5	C5	A6	C6
E	B1		B2		B3		B4		B5		B6	
F	B1		B2		B3		B4		B5		B6	
G	B1		B2		B3		B4		B5		B6	
H												

Appendix D

PRIMARY AND SECONDARY ANTIBODIES

Primary Antibody	Abbreviation	Dilution	Marker
Rabbit Anti-Cleaved Caspase 3	RbαCC3	1:100	Apoptosis
Mouse Anti-Prospero	MαPros	1:20	R7
Rat Anti-ELAV	RaαELAV	1:20	Pan-Neuronal (R1-R8)
Guinea Pig Anti-Senseless	GpαSen	1:1000	R8

Secondary Antibody	Abbreviation	Dilution	Fluorescence
Anti-Rabbit A^{488}	αRb A^{488}	1:500	Green
Anti-Mouse A^{564}	αM A^{564}	1:500	Red
Anti-Rat A^{647}	αRa A^{647}	1:500	Blue
Anti-Rat A^{488}	αRa A^{488}	1:500	Green
Anti-Guinea Pig A^{647}	αGp A^{647}	1:500	Blue

Appendix E

GENERATION OF THE RESCUE EXPERIMENT – *Drosophila* CROSSES

All females used in these crosses are virgins.

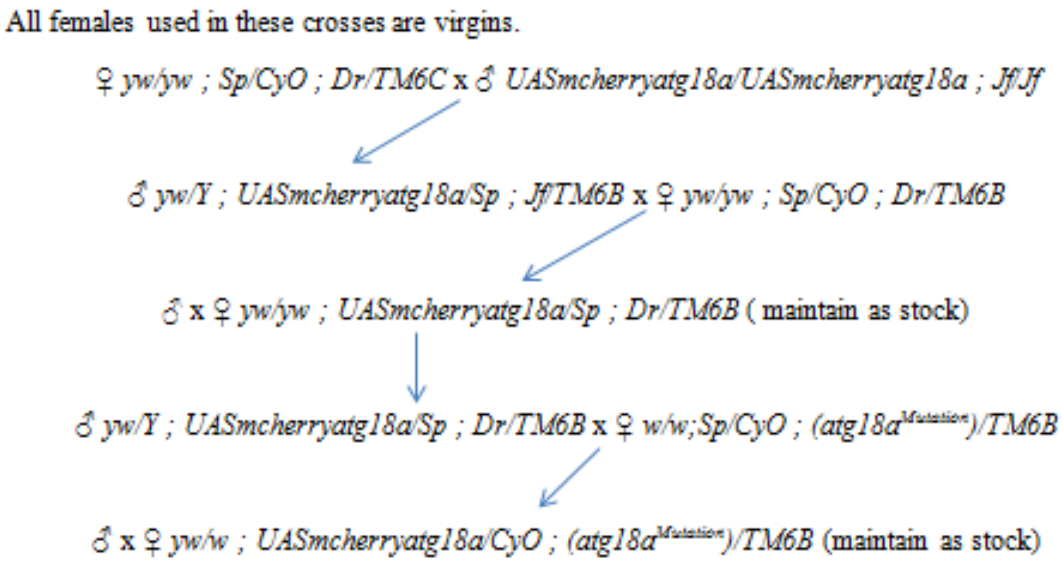

Experimental cross:

♀ *eyGal4:UASFLP/SM5 ; gmrhid$^{FRT\,2A}$/TM6B*

x

♂ *w/Y ; UASmcherryatg18a/CyO ; (atg18a^{Mutation})/TM6B*

Collect progeny and observe adult phenotypes to determine if rescue occurred:

Non-tubby, curly wings → Rescue phenotype (wildtype eyes)

Non-tubby, wildtype wings → Mutant phenotype; Small, rough eyes

Appendix F

qRT-PCR EXPERIMENTAL DATA

Transcriptional values were measured via qRT-PCR experiments using three different primer pairs; atg18 160F-287R, atg18 938F-1089R, and actin5C 332F-455R.

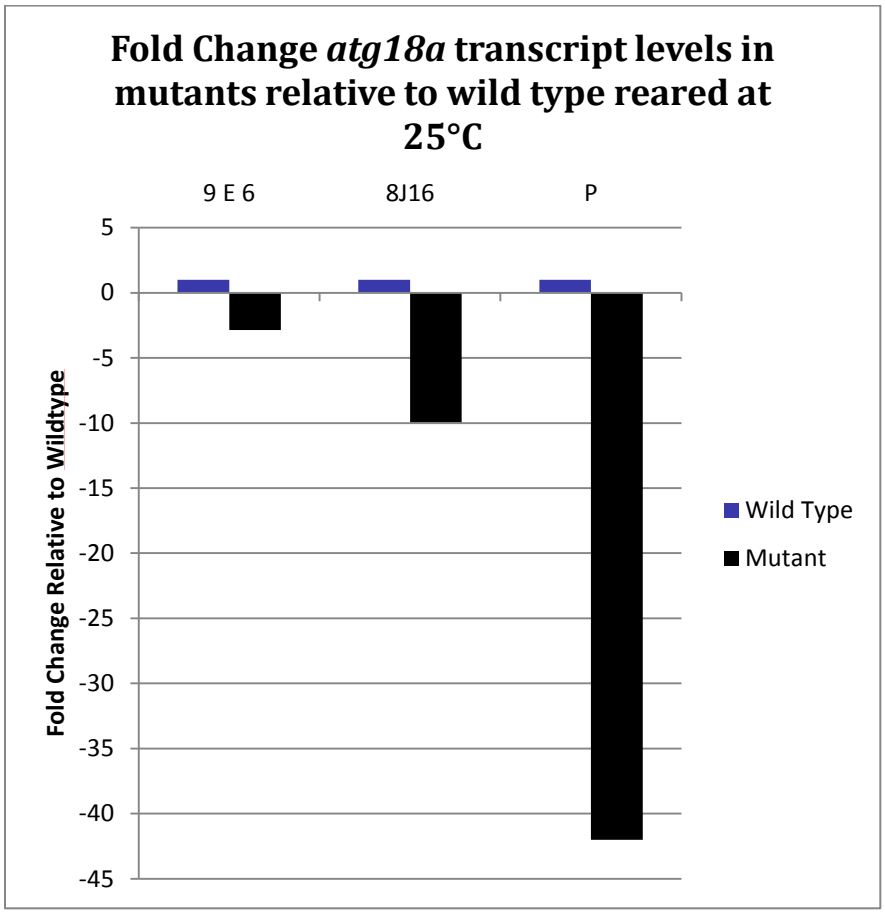

Changes in *atg18a* transcript levels in genotypes with respect to temperature